MucosalImmunology www.nature.com/mi

ARTICLE

IL-1β as mucosal vaccine adjuvant: the specific induction of tissue-resident memory T cells improves the heterosubtypic immunity against influenza A viruses

D. Lapuente[1,2], M. Storcksdieck genannt Bonsmann[1], A. Maaske[1], V. Stab[1], V. Heinecke[1], K. Watzstedt[1], R. Heß[1], A. M. Westendorf[3], W. Bayer[4], C. Ehrhardt[5] and M. Tenbusch[1,2]

A universal influenza vaccine must provide protection against antigenically divergent influenza viruses either through broadly neutralizing antibodies or cross-reactive T cells. Here, intranasal immunizations with recombinant adenoviral vectors (rAd) encoding hemagglutinin (HA) and nucleoprotein (NP) in combination with rAd-Interleukin-(IL)-1β or rAd-IL-18 were evaluated for their efficacy in BALB/c mice. Mucosal delivery of rAd-IL-1β enhanced HA-specific antibody responses including strain-specific neutralizing antibodies. Nevertheless, the beneficial effects on the local T cell responses were much more impressive reflected by increased numbers of $CD103^+CD69^+$ tissue-resident memory T cells (T_{RM}). This increased immunogenicity translated into superior protection against infections with homologous and heterologous strains including H1N1, pH1N1, H3N2, and H7N7. Inhibition of the egress of circulating T cells out of the lymph nodes during the heterologous infection had no impact on the degree of protection underscoring the unique potential of T_{RM} for the local containment of mucosal infections. The local co-expression of IL-1β and antigen lead to the activation of critical checkpoints in the formation of T_{RM} including activation of epithelial cells, expression of chemokines and adhesion molecules, recruitment of lung-derived $CD103^+$ DCs, and finally local T_{RM} imprinting. Given the importance of T_{RM}-mediated protection at mucosal barriers, this study has major implications for vaccine development.

Mucosal Immunology (2018) 11:1265–1278; https://doi.org/10.1038/s41385-018-0017-4

INTRODUCTION

Influenza viruses are the most common cause of severe viral respiratory tract infections leading to 250,000–500,000 deaths worldwide in an average flu season.[1] At present, the only influenza vaccines approved for all age groups are trivalent or quadrivalent inactivated influenza vaccines (TIV/QIV). These are designed to stimulate strain-specific neutralizing antibodies against the highly variable surface glycoproteins HA and neuraminidase. However, two major obstacles exist with these vaccines. On one hand, the overall vaccine efficacy is rather low with ~75 % and even lower in the high-risk group of the elderly.[2,3] On the other hand, the vaccine-induced antibodies confer protection solely against infections with influenza strains homologous to the vaccine. In seasons with substantial antigenic differences between vaccine and circulating strains, the vaccine efficacy against mismatched viruses can approach zero,[4] demonstrating the lack of heterosubtypic immunity (HSI) induced by TIV/QIV.

Compared to inactivated influenza vaccines, respiratory tract infections with influenza A viruses (IAV) induce a superior immunity, especially due to the establishment of mucosal immune responses including the secretion of immunoglobulin A (IgA) into the airways. Although still highly strain-specific, mucosal IgA is in a prime position to neutralize infectious virus before it crosses anatomical barriers and thereby exceeds the protective ability of IgG.[5] Furthermore, a moderate level of HSI is observed after resolving a natural IAV infection. This heterologous immunity is most likely mediated by cross-reactive T cell responses against highly conserved internal virus proteins, like NP, M1 and to a lesser extend M2.[6–8] Despite the fact that T cell-based HSI cannot prevent an initial infection, it reduces morbidity and mortality, as demonstrated extensively in mouse models[9–12] and more recently in humans.[13,14] Memory T cells circulate between lymphoid and non-lymphoid tissues but can also stably populate the lung mucosa as tissue-resident memory T cells.[15,16] Importantly, these T_{RM} mediate a rapid clearance of secondary IAV infections in mice and are essential for an optimal HSI.[16,17]

There are ample evidence showing that innate immune signaling via pattern-recognition receptors is indispensable for an efficient induction of adaptive immune responses during a primary IAV infection (reviewed by Iwasaki and Pillai).[18] Especially the activation of inflammasomes in the airway epithelium and concomitant mucosal production of IL-1β and IL-18 seems to be crucial for optimal antibody and T cell responses against IAV.[19,20] IL-1β is a hallmark cytokine of tissue inflammation[21] and attracts both innate and adaptive immune cells by the induction of chemokines and adhesion molecules,[19,20,22–24] but also has direct proliferative effects on $CD4^+$ and $CD8^+$ T cells.[25,26] Similarly, IL-18 mediates the chemoattraction of T cells,[27] influences their T_H1/T_H2

[1]Department of Molecular and Medical Virology, Ruhr-University Bochum, Bochum, Germany; [2]Institute of Clinical and Molecular Virology, University Hospital Erlangen, Friedrich-Alexander University Erlangen-Nürnberg, Erlangen, Germany; [3]Institute of Medical Microbiology, University Hospital Essen, University Duisburg-Essen, Essen, Germany; [4]Institute for Virology, University Hospital Essen, University Duisburg-Essen, Essen, Germany and [5]Institute of Virology, Westfaelische Wilhelms-University Muenster, Muenster, Germany Correspondence: M Tenbusch (matthias.tenbusch@fau.de)

Received: 24 July 2017 Revised: 19 January 2018 Accepted: 8 February 2018
Published online: 15 March 2018

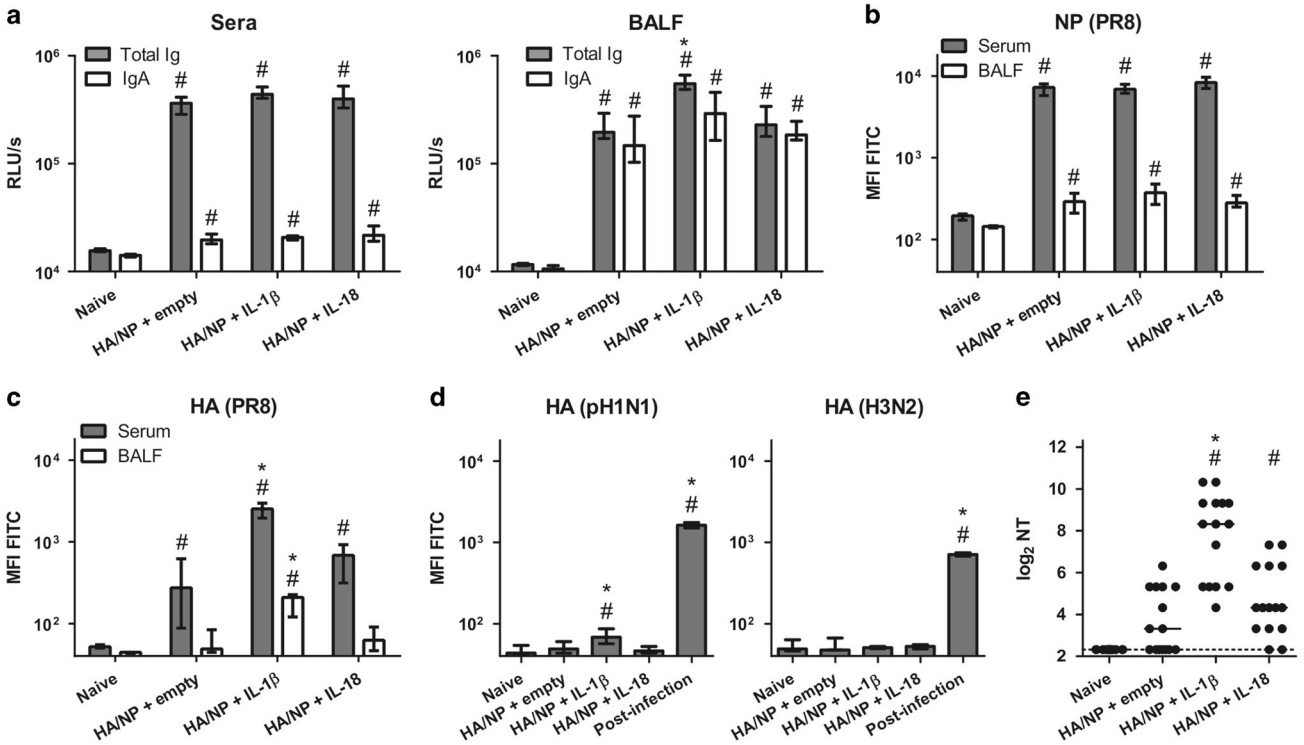

Fig. 1 Vaccine-induced antibody responses. BALB/c mice were immunized with 2×10^8 particles of rAd-HA and rAd-NP plus 1×10^9 particles of either rAd-empty, rAd-IL-18, or rAd-IL-1β. Serum and BALF were collected at day 42 and day 56, respectively. **a** Virus-specific total Ig and IgA in sera (1:10,000 dilution) and BALF (1:100 dilution) were analyzed in an ELISA coated with inactivated PR8. The median and interquartile range of the relative light units (RLU) is shown. **b**–**d** Flow cytometric analyses were performed with 293T cells expressing PR8 NP or HA (**b**, **c**; Sera 1:100, BALF 1:20) or HA derived from pH1N1 or H3N2 (**d**; Sera 1:20). Sera of mice recovered from sublethal pH1N1 or H3N2 infections were used as positive controls. The median MFI with the respective interquartile range is depicted per group. **e** Neutralizing antibodies against PR8 in sera were analyzed by microneutralization assay. Depicted are the neutralization titers (NT) of individual mice with the median of the group. The dotted line indicates the detection limit of NT = 5. Results represent eight to 12 mice per group for serum tests and seven to ten mice per group for BALF tests of two independent experiments. $^{\#}p < 0.05$ vs. naive; $^{*}p < 0.05$ vs. HA/NP + empty (data were log-transformed before analysis, one-way ANOVA, Tukey's post test)

Table 1. Amino acid identities between H1N1-derived vaccine components and heterologous influenza strains

Virus strain	Subtype	Identity HA	Identity NP
A/Puerto Rico/8/1934	H1N1		
A/Hamburg/4/2009	pH1N1	80.9 %	91.2 %
A/Hong Kong/1/1968	H3N2	41.3 %	93.6 %
A/Seal/Massachusetts/1/1980	H7N7	41.7 %	94.4 %

Amino acid sequences and respective alignments were retrieved from the Universal Protein Resource database (UniprotKB). UniProt identifiers for HA and NP proteins, respectively: H1N1 P03452 and P03466, pH1N1 C4RU35 and C4RU37, H3N2 Q91MA7 and P22435, H7N7 Q6LEJ4 and P26053. pH1N1, pandemic H1N1.

differentiation[28] and enhances proliferation of cytotoxic T cells (CTL).[29–32] Thus, Interleukin-1 family cytokines seem to be promising mucosal vaccine adjuvants as already proposed by others.[33]

To induce antigen and adjuvant expression in the relevant target tissue, we evaluated the co-delivery of vector-encoded IL-1β and IL-18 together with HA-encoding and NP-encoding adenoviral vectors in intranasal immunizations against IAV. We could demonstrate that the co-expression of IL-1β significantly increased the immunogenicity of our adenoviral vector vaccines especially in regard to the induction of mucosal responses. The specific establishment of cross-reactive T_{RM} also translated into improved HSI and provided protection against heterologous IAV strains.

RESULTS

rAd-IL-1β-adjuvanted immunization increases HA-specific antibody responses

BALB/c mice were immunized once intranasally with rAd-HA and rAd-NP (encoding the HA and NP derived from H1N1 A/Puerto Rico/8/1934; subsequently denoted PR8) together with rAd-IL-1β, rAd-IL-18, or an empty control vector (rAd-empty). The vaccine-induced antibody responses were analyzed in the serum 6 weeks later and in the bronchoalveolar lavage fluid (BALF) 8 weeks later (Fig. 1). All vaccinated mice developed substantial antigen-specific antibody responses as measured by ELISA using inactivated PR8 virus as coating agent. No significant differences were detected for total Ig and IgA in the sera, but, interestingly, the total Ig levels in BALF of animals that received the IL-1β-encoding vector were significantly higher than in the HA/NP + empty group (Fig. 1a). To gain insight about respective antibody specificities, we used cell lines expressing either NP or HA in their natural conformation and analyzed antibody binding in a FACS-based assay. Although we found no differences in the levels of total NP-specific antibodies among the immunized groups (Fig. 1b), HA-specific antibodies were significantly elevated in the serum and BALF of the HA/NP + IL-1β group (Fig. 1c). This was specifically true for antibodies of the subclass IgG1 (Fig. S1A+B). Cell lines expressing HA from heterologous IAV strains allowed us to study the breadth of the humoral response. In line with the decreasing homology among

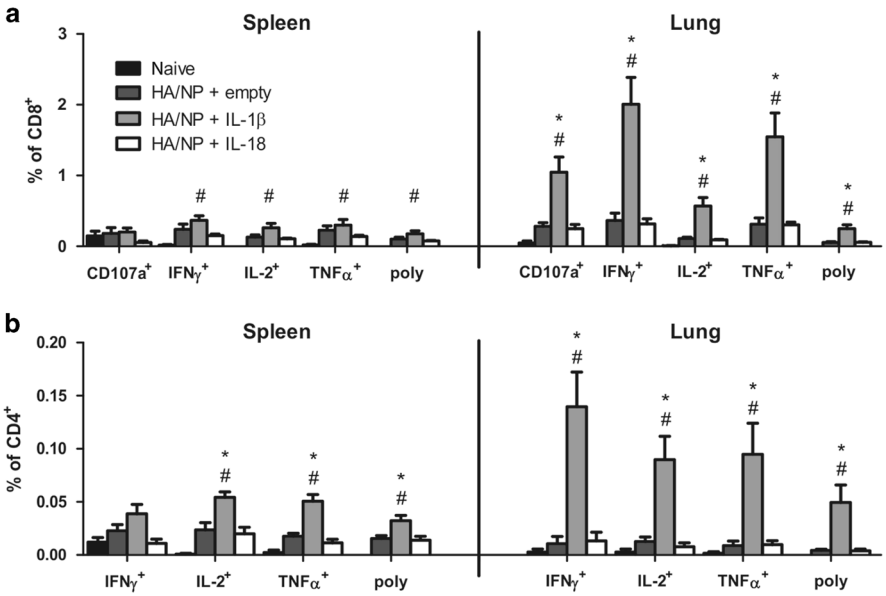

Fig. 2 Vaccine-induced T cell responses. BALB/c mice were immunized as described before. On day 56, intracellular cytokine staining was performed with lymphocytes isolated from the spleen and the lung. Cells were restimulated with MHC class I or II restricted peptides of NP. The frequencies of $CD8^+$ (**a**) and $CD4^+$ (**b**) T cells positive for the respective function or for all markers (poly; for $CD8^+$: $CD107a^+IFN\gamma^+IL\text{-}2^+TNF\alpha^+$; for $CD4^+$: $IFN\gamma^+IL\text{-}2^+TNF\alpha^+$) are shown. Mean values with standard error of the mean (SEM) represent data from four to six mice per group. $^{\#}p < 0.05$ vs. naive; $^{*}p < 0.05$ vs. HA/NP + empty (one-way ANOVA, Tukey's post test)

the HAs derived from PR8, pH1N1 and H3N2 (Table 1), low amounts of vaccine-induced antibodies were able to bind to the HA from pH1N1, but no cross-reactivity to the H3 variant was detected (Fig. 1d). In sharp contrast to the variability among different HA variants, NP shows a high identity among different IAV subtypes (Table 1), which explains the reactivity of immune sera in the ELISA using inactivated pH1N1 and H3N2 viruses as coating agent (Fig. S1C+D). In accordance with the narrow specificity of the HA-directed response, we observed neutralizing activity only against the homologous PR8 strain (Fig. 1e) but not against divergent pH1N1, H3N2 and H7N7 viruses (data not shown). Importantly, corresponding with the increased amount of HA-specific antibodies in the HA/NP + IL-1β group, we measured a 32-fold increased median neutralization titer in serum samples of mice from the HA/NP + IL-1β group compared to the HA/NP + empty group. Conclusively, the co-expression of IL-1β had a positive impact on the humoral response, whereas IL-18 had no significant effect.

rAd-IL-1β-adjuvanted immunization increases mucosal and systemic T cell responses

Internal IAV proteins like NP show a great identity among different IAV strains and therefore present an excellent target for the induction of cross-reactive T cell responses. To assess whether mucosally delivered IL-1β and IL-18 could enhance T cell responses, we isolated lymphocytes from spleen and lung tissues on day 56 post-immunization and restimulated these cells with immunodominant peptides from NP. Intracellular cytokine staining showed that all vaccine formulations induced $CD4^+$ and $CD8^+$ T cell responses toward NP (Fig. 2). However, while animals of the groups HA/NP + empty and HA/NP + IL-18 displayed only moderate responses, the inclusion of rAd-IL-1β in the vaccine formulation resulted in significantly higher frequencies of NP-specific, cytokine-secreting $CD8^+$ (Fig. 2a) and $CD4^+$ T cells (Fig. 2b). Although splenic responses showed the same trend, the beneficial effect of IL-1β co-expression was more prominent in the local response in the lungs. Here, the frequencies of IFNγ-secreting $CD4^+$ T cells increased 14-fold compared to the HA/NP + empty group (0.14 ± 0.03 % vs. 0.01 ± 0.006 %) and the responsive $IFN\gamma^+$ $CD8^+$ T cells were more than 5.5-fold elevated (2.01 ± 0.42 % vs. 0.36 ± 0.09 %). T cells producing other effector molecules like CD107a, IL-2, or TNFα as well as polyfunctional populations were similarly elevated (Fig. 2). Although overall at lower levels, the same enhancement was found for HA-specific T cell responses in the lungs (Fig. S2A+B). Again, IL-18 did not improve the T cell response compared to the non-adjuvanted group. Furthermore, in a separate experiment, we did not find elevated levels of IL-17-producing $CD4^+$ T cells, indicating no or only a minor impact of IL-1β expression on the induction of T_H17 cells in this vaccine setting (Fig. S2C).

rAd-IL-1β-adjuvanted immunization specifically induces lung T_{RM}

The mucosal administration of rAd-IL-1β led to strong T cell responses in the lung. It was tempting to speculate that these cells belong to the T_{RM} compartment, a memory phenotype persistent at mucosal linings and especially valuable in defending against respiratory pathogens like IAV.[16,17] Therefore, we analyzed the phenotype of the lung-derived T cells in more detail. First of all, the total number and the frequency of $CD8^+$ T cells were elevated in the lungs of immunized animals compared to naive mice with the highest values observed in the HA/NP + IL-1β group (Fig. 3a). Pentamer staining for $NP_{147–155}$-specific $CD8^+$ T cells revealed that the absolute number of these cells was 5.5-fold higher than in the HA/NP + empty group (1420 ± 329 cells vs. 259 ± 74 cells) and the relative contribution of these cells to the $CD8^+$ T cell population was also elevated (Fig. 3b).

Next, we used a combination of KLRG1 and CD127 to distinguish between effector T cells ($KLRG1^+CD127^-$, T_{EFF}) and effector memory T cells ($KLRG1^+CD127^+$, T_{EM}). $KLRG1^-$ memory cells were divided into CD69/CD103 single and double positive populations as potential T_{RM}. Finally, $KLRG1^-CD69^-CD103^-$ cells were classified as central memory cells (T_{CM}) based on their expression of CD127 (gating depicted in Fig. S3A). Overall, the numbers of potentially blood-derived, circulatory T_{EFF}, T_{EM}, and T_{CM} were rather low, but all subsets were slightly elevated in the HA/NP + IL-1β group (Fig. 3c). Different phenotypic occurrences of lung $CD8^+$ T_{RM} are described, but $CD103^+CD69^+$ seems to be the most stringent marker combination.[15–17,34] In our study,

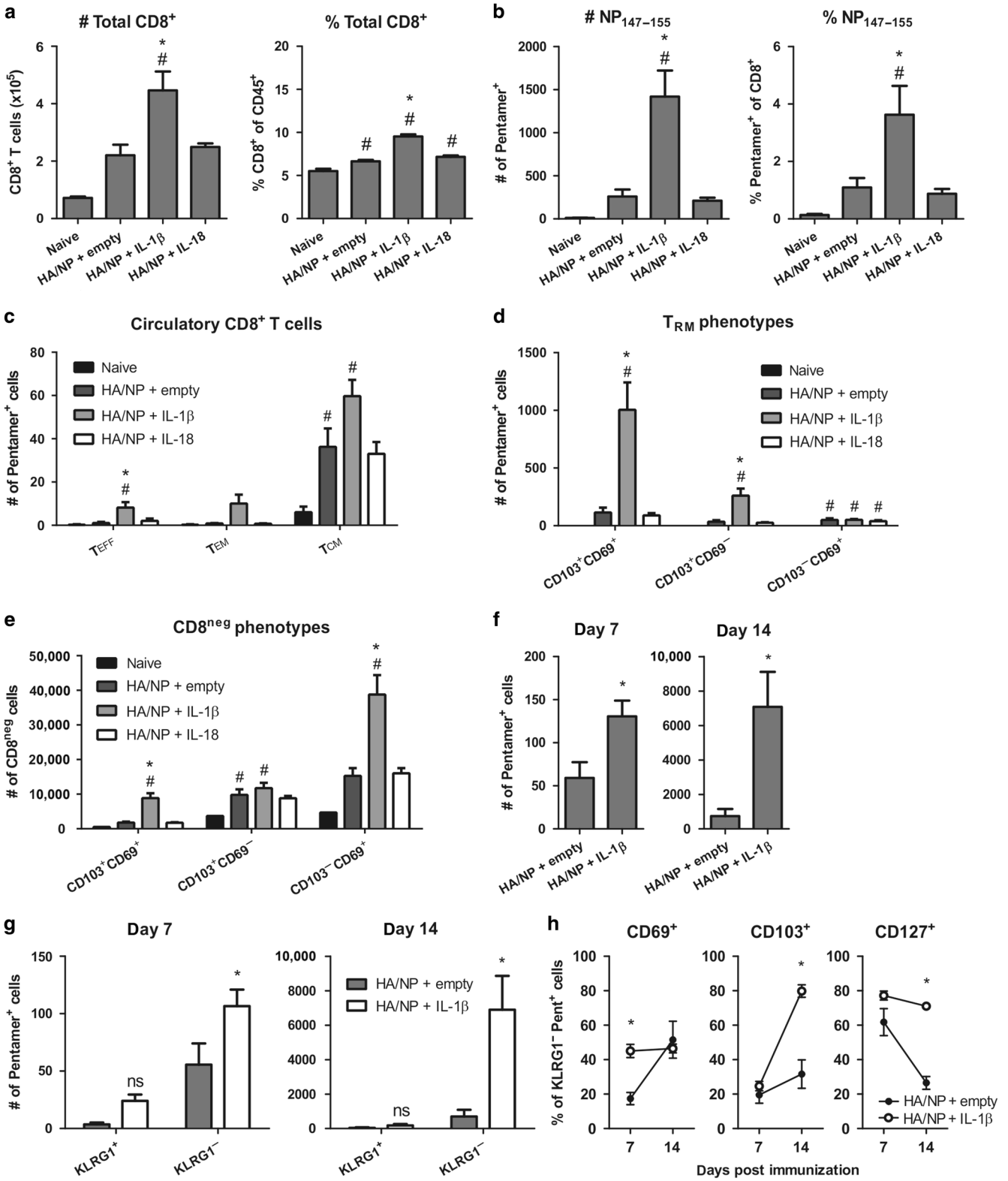

Fig. 3 Phenotypic characterization of lung-derived T cells. BALB/c mice were immunized as described before and lymphocytes from the lungs were analyzed by NP-specific pentamer staining on day 56. The numbers and frequencies of total (**a**) and NP-specific (**b**) $CD8^+$ T cells are shown. To distinguish the different memory populations within the pentamer$^+$ T cells, the expression of KLRG1, CD69, CD103, and CD127 was analyzed (gating shown in Fig. S3A). **c** Absolute numbers of pentamer$^+$ $CD8^+$ T cells are depicted for the different circulating memory subsets. **d** Potential T_{RM} subsets were identified by their expression of CD103 or CD69. **e** The T_{RM} phenotype was also investigated in the total CD8-negative lymphocyte population. **f** $NP_{147–155}$-specific $CD8^+$ T cells in the lung were analyzed at day 7 and day 14 after the immunization. **g** Antigen-specific cells were further divided into KLRG1$^+$ or KLRG1$^-$ cells. **h** $NP_{147–155}$-specific KLRG1$^-$ cells were analyzed regarding their expression of CD103, CD69, and CD127. Data represent four to six mice per group and time point. Curves and bars show the mean with SEM. $^{\#}p < 0.05$ vs. naive; $^{*}p < 0.05$ vs. HA/NP + empty (for **a**–**e**: one-way ANOVA, Tukey's post test; for **f**–**h**: two-tailed Student's *t*-test)

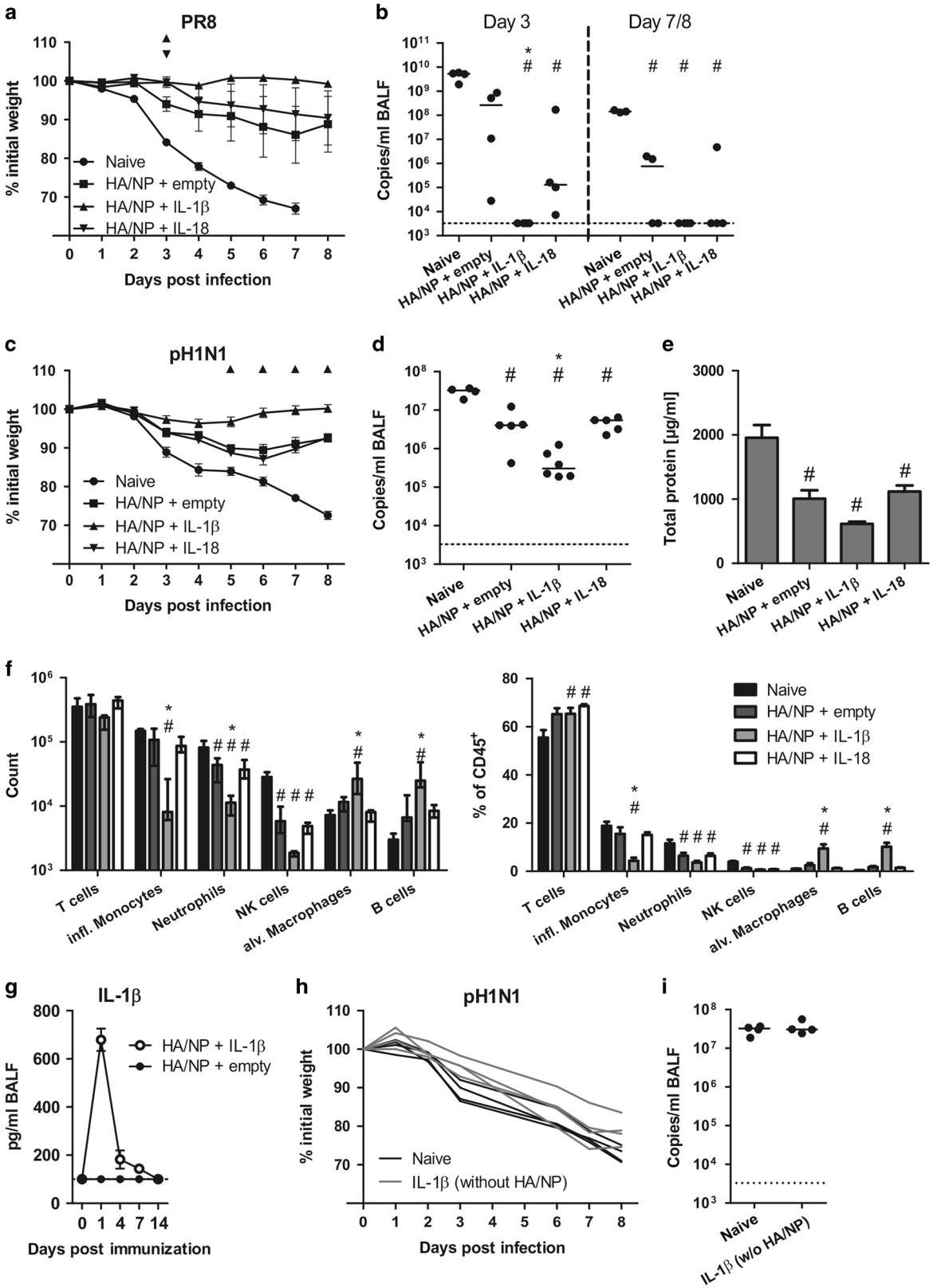

$CD103^+CD69^+$ cells were the predominant phenotype in the pool of $NP_{147–155}$-specific memory cells in lungs after the intranasal vaccination (Fig. 3d). Co-delivery of rAd-IL-1β induced a significant increase of this particular subset from an average number of 114 ± 38 cells in the HA/NP + empty group to 1004 ± 217 cells. Additionally, increased numbers of $CD103^+CD69^-$ cells were found. Intravascular staining with an anti-CD45.1 antibody clearly confirmed the tissue-residency of $CD103^+CD69^+$ and $CD103^-CD69^+$ cells, but 24 % of the $CD103^+CD69^-$ population were labeled by the injected antibody indicating that this

Fig. 4 Protective efficacy against infections with homologous and heterologous IAV strains. BALB/c mice were immunized as described before and infected with 10^4 PFU of either PR8 (**a**, **b**) or pH1N1 (**c**–**f**) on day 52. **a**, **c** Weight loss was monitored daily. **b** For the PR8 infection, four mice of each group were killed on day 3 and day 8 post-infection and viral loads in the BALF were analyzed by qRT-PCR. Naive animals were killed and analyzed already at day 7, because they reached the end-point criteria. The dashed line marks the detection limit (3300 copies/ml). **d** For the pH1N1 challenge, mice were killed 8 days post-infection and viral RNA copy numbers were quantified in the BALF. **e** The total amount of protein was determined in BALF of pH1N1-infected mice as a surrogate for tissue damage. **f** The cellular fraction of the BALF of pH1N1-infected mice was analyzed via multicolor flow cytometry. Absolute cell counts (left) and the relative contributions of the respective cell type within the $CD45^+$ compartment (right) are presented. alv. alveolar, infl. inflammatory. **g** Secreted IL-1β was determined in BALF at the indicated time points after the vaccination. Day zero indicates values of a naive group of mice. **h**, **i** Mice received solely 1×10^9 particles of rAd-IL-1β and were then infected with 10^4 PFU pH1N1 on day 52. Weight loss and viral RNA was analyzed as described above. Data represent three to eight mice and show the mean with SEM (**a**, **c**, **e**, **f** right, **g**), median with interquartile range (**f** left) or values of individual mice with the median of the group (**b**, **d**, **i**). $^{\#}p < 0.05$ vs. naive; * or the respective group sign, $p < 0.05$ vs. HA/NP + empty (data of **b** and **d** were log-transformed before analysis, one-way ANOVA, Tukey's post test)

phenotype does not exclusively contain T_{RM} (Fig. S3B). Interestingly, $CD103^{+/-}CD69^+$ cells in the CD8-negative lymphocyte population also demonstrated tissue-residency (Fig. S3B) and these specific phenotypes were significantly increased in rAd-IL-1β-treated mice (Fig. 3e). Thus, one can speculate that $CD4^+$ T cells, which normally account for approximately 30 % of the lymphocyte population in the lung, also show a bias toward tissue-residency.

We studied also the early induction of CTL and observed that already seven and 14 days after the immunization with rAd-IL-1β more antigen-specific CTL infiltrated the lung compared to the HA/NP + empty immunization (Fig. 3f). In both groups $KLRG1^-$ NP-specific cells were more abundant than terminally differentiated $KLRG1^+$ cells. However, the increase of antigen-specific $CD8^+$ T cells by rAd-IL-1β was mostly in the $KLRG1^-$ compartment (Fig. 3g), which represents potential T_{RM} precursors.[35] Moreover, NP-specific $KLRG1^-CD8^+$ T cells showed different phenotypic characteristics between both immunized groups (Fig. 3h). T cells from rAd-IL-1β-treated mice demonstrated an earlier upregulation of the activation marker CD69 and drastically elevated proportions of $CD103^+$ cells. Moreover, adjuvant treatment led to a more stable $CD127^+$ phenotype compared to non-adjuvanted mice.

rAd-IL-1β improves the vaccine efficacy against infections with homologous and heterologous IAV strains

Fifty-two days after the immunization, eight mice per group were infected with a high dose of the vaccine-homologous virus PR8 (10^4 plaque-forming units; PFU/~1000 median lethal dose; LD_{50}). Four animals of each group were killed either on day 3 or 8 (naive animals on day 7) to analyze viral RNA levels in the BALF. Starting from day 2, all non-immunized animals lost drastically weight and reached the end-point criteria on day 7 (Fig. 4a). In the groups HA/NP + empty and HA/NP + IL-18, the average weight loss was reduced, but substantial variation on the individual animal level could be detected. In contrast, none of the animals vaccinated with rAd-IL-1β showed any weight loss. These findings were reflected by the amount of viral RNA in the BALF (Fig. 4b). The naive animals demonstrated high viral titers at day 3 and 7 post-infection with a very low intergroup variance. Similarly, mice treated with HA/NP + empty or HA/NP + IL-18 showed initial viral replication on day 3, although in some animals at reduced levels. On day 7, at least half of the animals in these groups cleared the infection. However, viral RNA levels in the BALF of all rAd-IL-1β-treated animals were at both time points below the detection limit, indicating a sterile immunity in these animals. These results correlate with the variation seen for the neutralizing antibody titers in the different groups (Fig. 1e), which supports the notion that the protection against the infection with the homologous virus is mostly mediated by the HA-specific antibody response.

Next, we analyzed the efficacy against the heterologous pH1N1 A/Hamburg/4/2009 strain (10^4 PFU/~20 LD_{50}). As only minimal amounts of cross-reactive, non-neutralizing antibodies were observed, all animals showed signs of viral replication. Specifically, naive mice lost more than 25 % of their initial weight within 8 days, whereas the HA/NP + empty and the HA/NP + IL-18 groups showed a maximum average weight loss of 11 ± 1.3 % and 13 ± 1.4 % on day 6, respectively (Fig. 4c). In sharp contrast, the inclusion of rAd-IL-1β in the vaccine limited the maximum weight loss to 4 ± 1.1 % on day 4. Consequently, these mice recovered much faster than the ones from the other groups. Consistent with these weight curves, all vaccinated groups showed reduced levels of viral RNA (Fig. 4d) and total protein (surrogate for tissue damage, Fig. 4e) in BALF compared to naive mice. Importantly, the lowest levels were detected in the HA/NP + IL-1β group. Moreover, the analysis of the cellular infiltrate into the airways revealed significantly less infiltration of inflammatory monocytes and neutrophils, whereas alveolar macrophages and B cells were significantly increased compared to HA/NP + empty (Fig. 4f, gating strategy in Fig. S4A). By shifting the challenge infection to 100 days post-immunization, we also confirmed the long-term efficacy of the rAd-IL-1β containing vaccine, which still protected the animals from severe disease progression (Fig. S5A–D).

Furthermore, we excluded that an ongoing mucosal production of vector-encoded IL-1β influenced the immunity to pH1N1. We observed high levels of mucosal IL-1β 1 day after the immunization, but this expression waned within 7 days and was undetectable at day 14 (Fig. 4g). In addition, animals treated with rAd-IL-1β in the absence of rAd-HA/rAd-NP and infected with pH1N1 experienced weight loss (Fig. 4h) and viral replication (Fig. 4i) similar to non-immunized mice.

Next, we infected immunized mice with more distant, heterosubtypic IAV strains, namely the mouse-adapted H3N2 A/Hong Kong/1/1968 (10^4 PFU/~10 LD_{50}) or H7N7 A/Seal/Massachusetts/1/1980 (SC35M; 10^4 PFU/~40 LD_{50}). All vaccinated animals except one in the rAd-IL-18 treatment group survived the H3N2 infection, whereas all naive mice had reached the end-point criteria by day 8 (Fig. 5a). As seen in the pH1N1 challenge, the animals in the HA/NP + IL-1β group showed less severe disease progression and faster recovery than mice of the HA/NP + empty group. Specifically, the HA/NP + IL-1β group showed an average maximum weight loss of 8 ± 1.1 % on day 4 compared to a maximum weight loss of 22 ± 1.0 % in the HA/NP + empty group on day 6. Surprisingly, in this infection model rAd-IL-18-treated mice also showed a less severe disease progression compared to the HA/NP + empty group.

Revealing this strong adjuvant effect of rAd-IL-1β on the protection level, we titrated the dose of rAd-IL-1β in this challenge model while keeping the amount of antigen-expressing vectors constant. Indeed, a dose-dependent decline of the degree of protection could be observed in regard to weight loss, viral replication, and tissue damage (Fig. 5c–e). This is also paralleled with a dose-dependent decrease in the number of T_{RM} and cytokine-producing T cells (Fig. S6). Nevertheless, even a 100-fold reduction of rAd-IL-1β resulted in significantly less weight loss

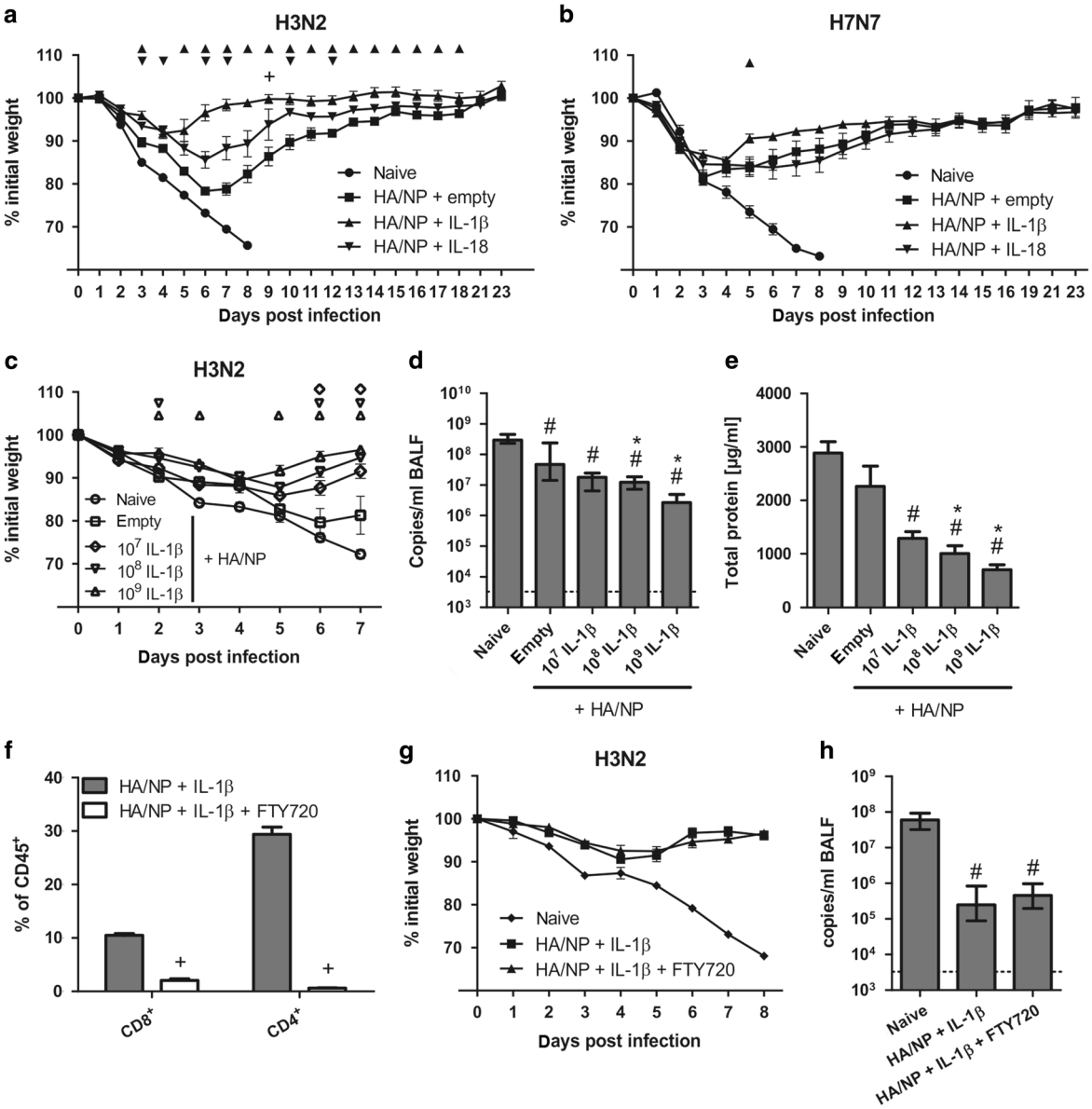

Fig. 5 T_{RM}-mediated protection against heterosubtypic IAV strains. BALB/c mice were immunized as described before and infected with 10^4 PFU of either H3N2 (**a**) or H7N7 (**b**) on day 52. **a**, **b** Weight loss upon infection was monitored daily and animals were killed when they reached the end-point criteria. This was the case for all naive mice on day 8 post-infection at the latest and for one animal of the IL-18 group, which was infected with H3N2, on day 9 (as indicated by +). **c**–**e** BALB/c mice were immunized with 2×10^8 particles of rAd-HA and rAd-NP plus 10^9 particles rAd-empty or the indicated amount of rAd-IL-1β. On day 52, mice were infected with 10^4 PFU of H3N2 and killed 7 days post-infection. Viral RNA copy numbers (**d**) and the total amount of protein (**e**) was determined in BALF. **f**–**h** Three groups of mice were infected with H3N2 as described above. One group of mice was unvaccinated and two groups got rAd-HA/NP and rAd-IL-1β as in the previous experiments. Mice in one of the vaccinated groups got daily injections of FTY720 (1 mg/kg i.p.), which began 3 days before infection and were continued throughout the challenge to inhibit circulation of T cells. Mice were killed and BALF as well as PBMCs were obtained on day 8 post-infection. **f** The frequency of circulating T cells in PBMCs was determined via flow cytometry. **g** Weight loss was monitored daily. **h** BALF were analyzed for viral RNA. Data represent seven mice per group in **a** and four to six mice in **b**–**h**. Curves and bars show the mean with SEM (**a**–**c**, **e**–**g**) or median with interquartile range (**d**, **h**). $^{\#}p < 0.05$ vs. naive; * or the respective group sign, $p < 0.05$ vs. HA/NP + empty; $^{+}p < 0.05$ vs. HA/NP + IL-1β (for **a**–**e** and **g**, **h**: values of **d**, **h** were log-transformed before analysis, one-way ANOVA, Tukey's post test; for **f**: two-tailed Student's *t*-test)

after the heterologous infection compared to the non-adjuvanted vaccine demonstrating the potency of rAd-IL-1β. Our vaccines were also fully protective against a high dose (40 LD_{50}) of a seal-origin H7N7 virus (Fig. 5b). Probably due to the high challenge dose, the adjuvant effect of IL-1β was less impressive but still visible by the reduced weight loss. Thus, these results demonstrate that the vaccine establishes a broad protection against distant IAV subtypes and that this protection can be enhanced even by low doses of rAd-IL-1β as genetic adjuvant.

Heterosubtypic immunity mediated by HA/NP + IL-1β protects independent of systemic T cell responses

To prove that the increased lung-resident memory T cell population in the HA/NP + IL-1β group is sufficient to provide heterosubtypic protection, we treated a group of rAd-IL-1β-immunized mice with FTY720 before and during the infection with the H3N2 virus. This chemical binds to sphingosine-1-phosphate receptors and inhibits the ability of T cells to leave lymphatic tissues.[36] The treatment led to an almost complete absence of

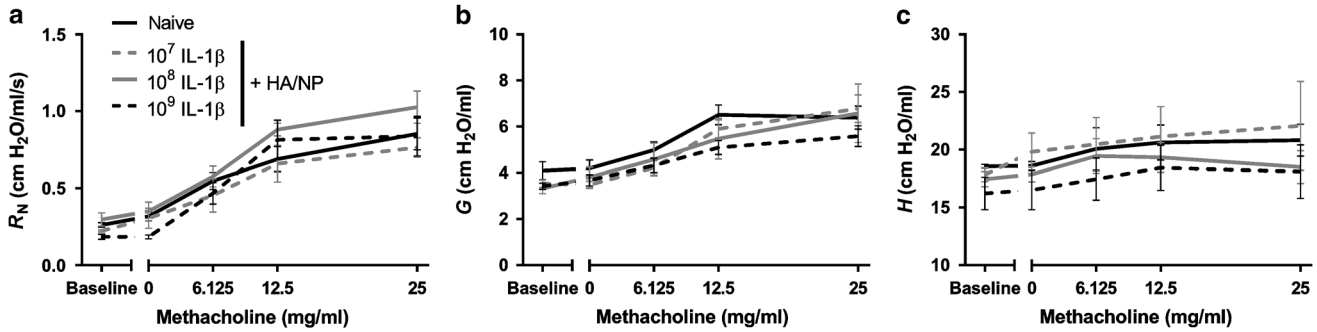

Fig. 6 Assessment of the lung function. BALB/c mice were immunized with 2×10^8 particles of rAd-HA and rAd-NP plus increasing doses of rAd-IL-1β. Three days later, mice were anesthetized and the trachea canulated and connected to a ventilation device. Animals were exposed to increasing concentrations of vaporized methacholine. The baseline data were recorded without any vaporization, whereas "0" indicates the vaporization of the vehicle (PBS). Forced oscillation maneuvers were performed to measure the airway resistance R_N (**a**), tissue damping G (**b**), and tissue elastance H (**c**). Depicted are the respective parameters plotted against the vaporized methacholine concentration. Data are represented as means + SEM and statistical significances were analyzed by one-way ANOVA followed by Tukey's post test ($n = 3$–4; no statistically significant differences observed)

circulating T cells in the blood as confirmed by FACS analysis of PBMCs (Fig. 5f). Impressively, compared to immunized mice with circulating memory T cells, the FTY720-treated animals displayed highly similar weight curves (Fig. 5g) and viral replication (Fig. 5h). This indicates that lung-resident memory T cells are sufficient for the heterosubtypic protection.

The mucosal expression of IL-1β is sufficient to start a coordinated inflammatory program including crucial mediators of T_{RM} formation

As IL-1β is a potent cytokine that can induce lung injury at high doses,[37,38] we monitored the health status and the inflammatory response early after immunization. Indeed, animals vaccinated with the high dose (10^9 particles) of rAd-IL-1β showed moderate side effects like ruffled fur and reduced activity, which typically normalized 3 to 4 days after the vaccination. This mirrors the transient expression of IL-1β shown in Fig. 4g. Nevertheless, to exclude severe lung injury and impaired gas exchange, we measured the lung function via forced oscillation technique with inhalation of escalating doses of the bronchoconstrictor methacholine as an aerosol.[39] None of the tested doses of rAd-IL-1β resulted in an increase of airway resistance, tissue damping or tissue elastance (Fig. 6) compared to non-vaccinated animals. To characterize the inflammatory response induced by the instillation of rAd-IL-1β, we monitored the cellular infiltration and the cytokine/chemokine profile in the lungs at early time points after the vaccination compared to rAd-empty (Fig. 7 and 8). Most probably as a direct consequence of an activation of the lung epithelium by IL-1β, the pro-inflammatory cytokines IL-6 and TNFα as well as the chemokines CCL3, CCL5, and CCL20 could be detected already 1 day post-infection in the BALF (Fig. 7a–e). Furthermore, the upregulation of adhesion molecules measured by elevated transcription of the selectin genes *Selp* and *Sele* allowed for transendothelial migration of immune cells (Fig. 7f, g). In accordance to the high levels of the neutrophil-attracting chemokine CXCL1 (Fig. 7h), a massive influx of neutrophils started already 1 day after immunization and was followed by migrating monocytes and respiratory $CD11b^+$ DCs on day 4 (Fig. 8). At the same time, a massive recruitment of $CD103^+$ DCs started. Specifically, a 50-fold increase was observed from around 220 ± 30 cells at baseline to 11,600 ± 230 cells at the end of the observation period. Adaptive immune cells, namely $CD4^+$ and $CD8^+$ T cells as well as $CD19^+$ B cells, started to infiltrate the lung at day 7 and further expanded until day 14 after the immunization (Fig. 8). This was paralleled by the detection of a second panel of cytokines, probably produced by recruited monocytes or DCs. These factors included the chemokines CCL21, CXCL10, and CXCL12 (Fig. 7i–k), as well as the cytokines TGFβ, IL-17, and B cell activating factor of the TNF family (BAFF; Fig. 7l–n).

Importantly, CXCL10 and TGFβ are described as mandatory for the infiltration of $KLRG1^-$ T_{RM} precursors and the induction of CD103 expression, respectively.[35,40] This fits very well to our data on the early NP-specific $CD8^+$ T cell response presented in Fig. 3f–h. Finally, we detected elevated *Vcam1* mRNA levels 14 days after immunization in the lungs of rAd-IL-1β-treated animals (Fig. 7o), which might indicate the onset of an antiviral state triggered by the primary T_{RM} response.[41]

Furthermore, the local antigen expression was a prerequisite for the final imprinting of the T_{RM} phenotype, as the IL-1β-induced lung inflammation was not sufficient to develop substantial numbers of NP-specific T_{RM} in the absence of local antigen (Fig. 9a–c). When the antigens were delivered intramuscularly and the rAd-IL-1β was given intranasally, NP-specific T cells were recruited into the lung but displayed mainly an effector or effector memory phenotype. In accordance, highly polyfunctional $CD8^+$ and $CD4^+$ T cells were found at significantly higher numbers if both vectors were applied mucosally (Fig. 9d, e). Lastly, using rAd-IL-1β as adjuvant in a solely intramuscular schedule did not substantially improve the mucosal T cell response demonstrating the specificity as mucosal adjuvant (Fig. 9).

DISCUSSION

As the efficacies of seasonal inactivated influenza vaccines are rather low and limited to closely matched strains, alternative platforms are currently being tested to improve particularly the breadth of the protection provided by the vaccine.[42] From natural infections it is known that mucosal immune responses are strong correlates of protection[5,16] and that especially cellular immune responses against highly conserved structural proteins can mediate HSI against divergent IAV strains.[13,14,43] Several studies revealed that adenoviral vectors are among the most potent vaccine platforms to induce cellular responses.[44–47] In the present study, intranasal immunizations with HA-encoding and NP-encoding adenoviral vectors induced substantial protection against infections with homologous as well as heterologous IAV strains, which could be significantly improved by the co-delivery of vector-encoded IL-1β but not by IL-18. Although both cytokines belong to the same family and have in part quite similar properties,[48] there are still differences in the induced signaling pathways. In line with previous reports,[49] our rAd-IL-18 is less potent in in vitro reporter assays to stimulate the NF-κB pathway, but nearly comparable to rAd-IL-1β in the stimulation of AP-1 or IFNβ (Fig. S7). Furthermore, IL-1β generally possesses a higher

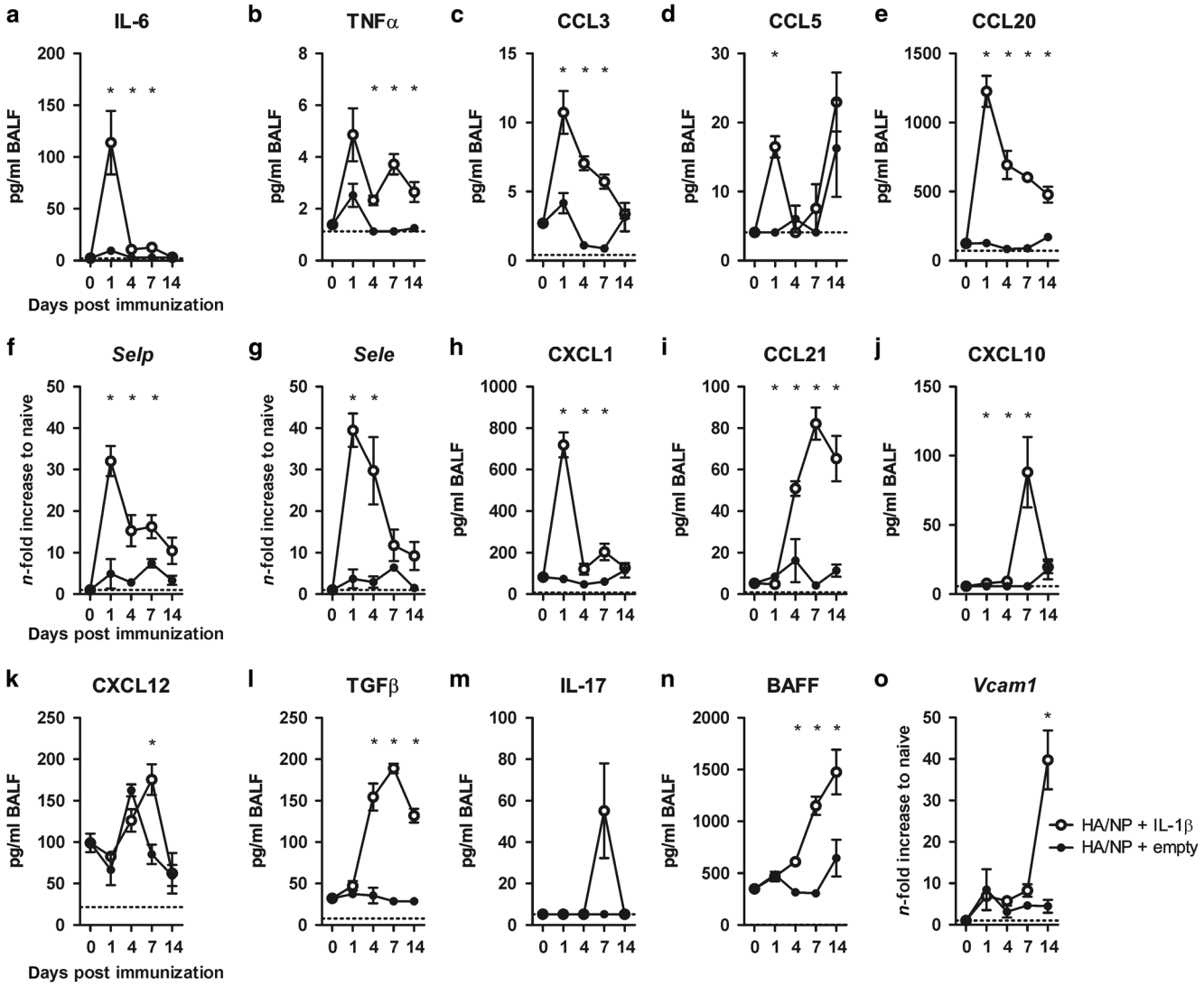

Fig. 7 Kinetics of pro-inflammatory cytokines and chemokines. **a**–**e**, **h**–**n** Chemokines and cytokines in BALF were measured at the indicated time points after the vaccination via bead-based multiplex analysis and ELISA. Day zero indicates values of the same naive group of mice for both curves (HA/NP + empty and HA/NP + IL-1β). **f**, **g**, **o** *Selp*, *Sele*, and *Vcam1* mRNA levels were analyzed via qRT-PCR analysis of lung tissue preparations at the indicated time points. Transcriptional levels were normalized via quantification of the reference genes *ubiquitin c* and *eukaryotic elongation factor 2* and are shown as relative increases to the naive steady state. Dotted lines represent detection limits. Data derive from four mice per group and time point. Curves show the mean with SEM. *$p < 0.05$ vs. HA/NP + empty (two-tailed Student's *t*-test)

bioactivity than IL-18[50] and is known to induce the upregulation of adhesion molecules on endothelial cells,[21] which might be an important feature for the adjuvant effect as explained below.

IL-1β-treated animals were the only ones showing sterile immunity to the homologous virus PR8, which correlates with the stronger HA-specific antibody responses in this group including strain-specific neutralization. This enhancing effect on systemic as well as mucosal humoral responses had been also reported for intranasal protein immunizations with recombinant HA and IL-1β or other IL-1 superfamily members.[33] But surprisingly, the antibody response to the NP antigen was not affected by the co-expression of IL-1β in our study suggesting that the antigen localization is important for the resulting B cell response. Nevertheless, due to the tight strain-specificity of the HA antibodies and the comparable levels of NP-specific antibodies in all vaccine groups, antibody-mediated mechanisms are rather unlikely to contribute to the superior protection against heterologous IAV infections. As demonstrated also by others, T cell responses against the conserved NP induced by vaccination or natural infection can confer partially HSI in animals[9–12] and humans.[13,14] Here we show for the first time, that mucosal expression of IL-1β can specifically enhance local $CD4^+$ and $CD8^+$ T cell responses in the lung, which correlates with superior control of heterologous IAV infections.

Interestingly, we observed that rAd-IL-1β had a much stronger impact on the initiation of mucosal T cells than on systemic responses. The adjuvant specifically induced $CD103^{+/-}CD69^+$ lung-resident $CD8^+$ T cells. As early as 7 days post-immunization, potential $KLRG1^-CD8^+$ T_{RM} precursors could be isolated from the lung with increased expression of the C-type lectin CD69 and CD103 (α chain of integrin $\alpha_E\beta_7$), yet the most reliable markers for lung-resident $CD8^+$ T cells in mice.[15–17,34,51] However, in our studies also CD8-negative cells showed an enriched T_{RM} phenotype, which might indicate that also $CD4^+$ T cells experienced an improved T_{RM} imprinting upon rAd-IL-1β treatment. $CD4^+$ T cells can persist locally in the lung as well and contribute to the immunity against heterologous IAV.[52,53] Confirmed by ICS, both $CD4^+$ and $CD8^+$ T cells isolated from the lung were highly

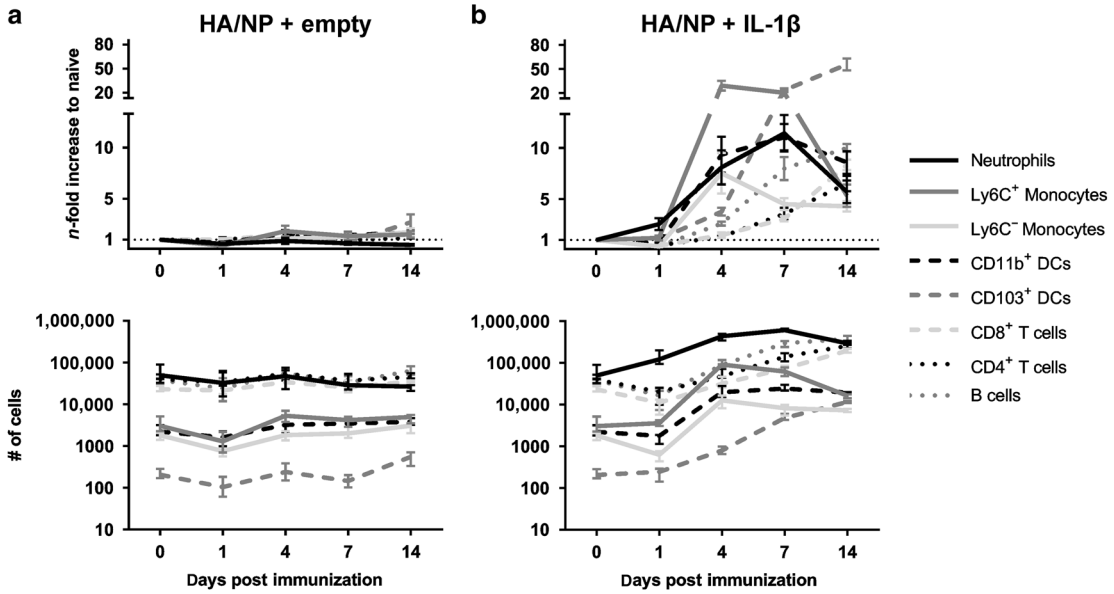

Fig. 8 Kinetics of cellular infiltration. **a**, **b** BALB/c mice were immunized with 2×10^8 particles of rAd-HA and rAd-NP plus 1×10^9 particles of either rAd-empty (**a**) or rAd-IL-1β (**b**). Lungs were harvested at the indicated time points after the immunization and single cell preparations were analyzed via multicolor flow cytometry (gating see Fig. S4B+C). One group of naive mice ($n = 4$) was used to determine the steady state in the lung (day 0). The lower graphs illustrate the total numbers of several infiltrating immune cell subsets, while the upper graphs show the relative increases compared to the naive steady state. Curves represent the mean with SEM (top) or median with interquartile range (bottom)

functional after antigen-specific restimulation. Furthermore, treatment with FTY720 to block the egress of T cells from the lymph nodes did not reduce the protective capacity of our vaccination approach indicating that tissue-resident memory T cells are sufficient to immediately control viral replication at the mucosal entry side. This is in line with previous reports on the protective role of T_{RM} in secondary IAV infections.[16,17]

Our study provides evidence that local antigen presentation and IL-1β-induced tissue activation are both required for the recruitment of T_{RM} precursor cells into the tissue and the final imprinting of a resident memory phenotype. Mechanistically, we hypothesize that early tissue activation by IL-1β results in the upregulation of adhesion molecules in concert with chemokine expression. This allows the efficient transendothelial migration of innate immune cells (i.a., neutrophils), which is in line with earlier reports on the function of IL-1β.[54,55] Especially the recruitment of antigen-presenting cells and in particular $CD103^+$ DCs has been described to be essential for the efficient induction for T_{RM}.[20,56] In the present study, rAd-IL-1β induced $CD103^+$ DCs together with high amounts of CXCL10, a chemotactic ligand for CXCR3 on $KLRG1^-$ T_{RM} precursors.[35] Finally, T_{RM} phenotype imprinting is highly dependent on tissue instruction. In addition to several other cytokines, we observed high levels of local TGFβ, which is essential in CD103 upregulation on T_{RM}.[35] Moreover, we hypothesize that the high amount of local CCL21 might counteract the CCR7-mediated tissue egress and thus contributes to the retention of T_{RM}.[35] With regard to the short duration of the IL-1β expression, this might indicate that IL-1β is rather starting a coordinated inflammatory process generating the optimal environment for T_{RM} induction than acting directly on the T cells via IL-1R signaling. Since there are contradictory reports on the role of IL-1R signaling on the induction of lung CTL,[20,26] this should be further analyzed in detail for our vaccination approach in appropriate bone-marrow chimeras. However, mucosal inflammation induced by IL-1β alone was not sufficient to differentiate antigen-experienced T cells into T_{RM}, which indicates differences in the requirements for tissue-residency of T cells in the lung and other tissues.[57,58] Furthermore, applying rAd-IL-1β as an adjuvant in intramuscular regimens had no impact on the mucosal immunity as well. This is in line with our earlier study, in which intramuscular DNA immunizations with NP-encoding and IL-1β-encoding plasmids demonstrated no measurable impact of the adjuvant on the T cell response (Master´s thesis D. Lapuente, 2013).

Acute lung injury and fibrosis had been reported upon intranasal delivery of high doses of rAd-IL-1β to mice or rats,[37,38] which might raise concern about the use of Interleukin-1β as adjuvant. Importantly, also during natural infections transiently elevated levels of IL-1β occur and patients normally recover without long-lasting lung injury. Furthermore, some lung injury and tissue repair even seem to be a prerequisite for the successful establishment and retention of $CD8^+$ T_{RM} in the lungs after an IAV infection, as recently described by Takamura et al.[59] However, in our experiments we did not observe any signs of long-term lung injury for all doses tested. This is further supported by the fact that rAd-IL-1β-treated animals had no complications during infection.

Therefore, our vaccination approach combines the local antigen expression and inflammation that are needed for the efficient induction of lung-resident memory T cells. Together with the enhanced mucosal antibody response, this immunity mediates protection against four distantly related IAV strains, namely H1N1, pH1N1, H3N2, and H7N7, indicating the potential for a universal flu vaccine.

METHODS

Adenoviral vectors

Replication-deficient (ΔE1ΔE3) rAd serotype 5 vaccine and adjuvant vectors were produced according to the pAdEasy protocol.[60] Briefly, codon-optimized gene sequences for hemagglutinin and nucleoprotein, both derived from H1N1 A/Puerto Rico/8/1934, as well as the sequences for murine mature IL-1β and IL-18 were cloned into pShuttle. The leader peptide of the tissue plasminogen activator was added at the N terminus to allow efficient secretion of the cytokines and all transgenes contain an OLLAS tag at the C terminus.[61] A vector lacking transgene expression (rAd-empty) was obtained by homologous

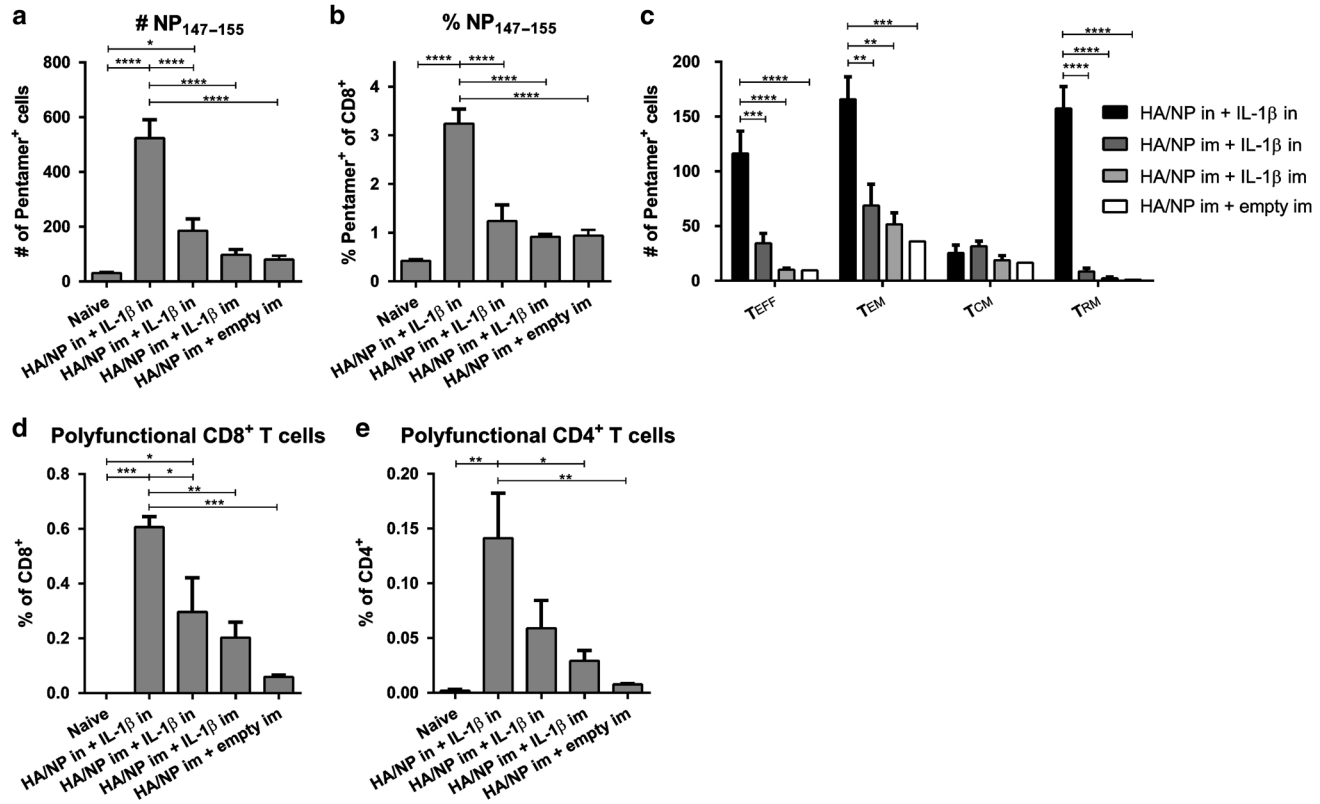

Fig. 9 Induction of T_{RM} by different routes of immunization. BALB/c mice were immunized with 2×10^8 particles of rAd-HA and rAd-NP plus 1×10^9 particles of either rAd-empty or rAd-IL-1β via the indicated route (in = intranasal; im = intramuscular). Lymphocytes from the lungs were analyzed by NP-specific pentamer staining on day 56. The numbers (**a**) and frequencies (**b**) of pentamer$^+$ cells are shown. **c** Different memory populations within the pentamer$^+$ T cells were analyzed as described earlier (T_{RM} refers to CD103$^+$CD69$^+$ T cells). Intracellular cytokine staining for NP-specific CD8$^+$ (**d**) and CD4$^+$ T cells (**e**) was performed with lung lymphocytes as described earlier. Polyfunctional T cells positive for all measured markers (for CD8$^+$: CD107a$^+$IFNγ$^+$IL-2$^+$TNFα$^+$; for CD4$^+$: IFNγ$^+$IL-2$^+$TNFα$^+$) are shown. Data represent four mice per group and show the mean with SEM. *$p < 0.05$; **$p < 0.01$; ***$p < 0.001$; *****$p < 0.0001$ (one-way ANOVA, Tukey's post test)

recombination of pShuttle-CMV with pAdEasy-1. Viral particles were purified with the Vivapure AdenoPack kit (Sartorius). The concentration of total rAd was measured by optical density at 260 nm and infectious particles by Reed-and-Muench $TCID_{50}$.[62] Ratios of total to infectious particles usually were in the range of 200:1. The integrity of the expression cassettes was confirmed by PCR and transgene expression was detected by Western blot. Endotoxin levels were measured by QCL-1000 Chromogenic LAL assay (Lonza; all preparations <0.0001 endotoxin units/immunization dose).

Mice and immunizations

Six to eight-weeks-old female BALB/cJRj mice were purchased from Janvier (Le Genest-Saint-Isle, France) and housed in individually ventilated cages in accordance with German law and institutional guidelines. The study was approved by an external ethics committee authorized by the North Rhine-Westphalia State Office for Consumer Protection and Food Safety and performed under the project license AZ 84-02.04.2013-A371. Mice were immunized intranasally (or intramuscularly in indicated experiments) with a dose of 2×10^8 particles of each antigen-encoding vector in combination with 1×10^9 particles encoding the adjuvant (unless stated otherwise). The vaccine was slowly pipetted into one nostril under general anesthesia (100 mg/kg ketamine and 15 mg/kg xylazine). Blood samples were collected from the retro-orbital sinus under light anesthesia with inhaled isoflurane. For analysis of mucosal immune responses, animals were killed with an overdose of inhaled isoflurane, the tracheae were canulated and BALF were collected by rinsing the lungs twice with 1 ml cold PBS. Subsequently, lungs and spleens were removed.

Antigen-specific antibody ELISA

Ninety-six-well ELISA plates were coated with 5×10^5 PFU heat-inactivated influenza particles per well diluted in carbonate buffer overnight at 4 °C. Afterwards, free binding sites were blocked with 5 % skimmed milk in PBS-$T_{0.05}$ containing 0.05 % Tween-20. After a washing step with PBS-$T_{0.05}$, diluted sera or BALF were added and incubated for 1 h. Subsequently, plates were washed and HRP-coupled polyclonal anti-mouse Ig (P0260, Dako) or anti-mouse IgA (A90-103P, Bethyl Laboratories) detection antibodies were added for 1 h. After a final wash with PBS-$T_{0.05}$ and the addition of an ECL substrate, the signals were detected with a microplate luminometer (Orion L, Titertek Berthold).

FACS-based antibody analysis

The flow cytometric antibody analysis was conducted as described elsewhere.[63] Briefly, HEK 293T cells were transfected with plasmid DNA encoding the antigen of interest together with plasmids encoding a fluorescent protein (dsRed or BFP). Forty-eight hours post-transfection, the cells were incubated with sera or BALF diluted in FACS-PBS (PBS with 0.5 % BSA and 1 mM sodium azide) to bind to HA on the surface, or diluted in permeabilization buffer (0.5 % saponin in FACS-PBS) to bind to intracellular NP. Afterwards, specifically bound antibodies were detected with polyclonal anti-mouse Ig-FITC, anti-mouse IgG1-APC (clone X56), or anti-mouse IgG2a-FITC (clone R19-15, all BD Biosciences). The median FITC or APC fluorescence intensity of transfected cells (dsRed$^+$ or BFP$^+$)

was measured on a BD FACSCanto™ II and analyzed using FlowJo™ software (Tree Star Inc.).

Influenza microneutralization assay

To determine influenza-specific neutralizing antibody titers, a microneutralization assay was performed as previously described.[64] In short, two-fold serial dilutions of serum samples were incubated with 2000 PFU influenza. Afterwards, each serum-virus mix was added to confluent MDCK II cells in a 96-well plate. Four days later, plaques were identified by crystal violet staining. The highest reciprocal sample dilution, which completely inhibited an infection, was considered as the neutralization titer.

Intracellular cytokine staining

At the indicated time points, animals were killed to isolate lymphocytes from lung and spleen tissue. Lung tissue was cut into small pieces and treated for 45 min at 37 °C with 500 units Collagenase D and 160 units DNase I in 2 ml R10 medium (RPMI 1640 supplemented with 10 % FCS, 2 mM L-Glutamine, 10 mM HEPES, 50 µM β-mercaptoethanol and 1 % penicillin/streptomycin). Digested lung tissues and spleens were mashed through a 70 µm cell strainer before the suspensions were subjected to an ammonium-chloride-potassium lysis. 10^6 splenocytes or one fifth of the total lung cell suspension were plated per well in a 96-well round-bottom plate and incubated for 6 h in 200 µl R10 medium containing monensin (2 µM), anti-CD28 (1 µg/ml, eBioscience), anti-CD107a-FITC (clone eBio1D4B, eBioscience) and 5 µg/ml of the peptides $HA_{110–120}$ (SFERFEIFPKE), $HA_{518–526}$ (IYSTVASSL), $NP_{55–69}$ (RLIQNSLTIERMVL), or $NP_{147–155}$ (TYQRTRALV), respectively. Non-stimulated samples were used for subtraction of background cytokine production (negative values were set as zero). After the stimulation, cells were stained with anti-CD8a-Pacific blue (clone 53-6.7, BD Biosciences), anti-CD4-PerCP (clone RM4-5, eBioscience) and Fixable Viability Dye eFluor® 780 (eBioscience). After fixation and permeabilization, cells were stained intracellularly with anti-IL-2-APC (clone JES6-5H4, BD Biosciences), anti-TNFα-PECy7 (clone MPG-XT22, BD Biosciences), and anti-IFNy-PE (clone XMG1.2, eBioscience). Data were acquired on a BD FACSCanto™ II and analyzed using FlowJo™ software (Tree Star Inc.).

Pentamer and intravascular staining

Lymphocytes were isolated from lung tissue as described above. One fifth of the cell suspension was incubated with APC-labeled H-$2K^D$ $NP_{147-155}$ pentamer (ProImmune) for 20 min at 4 °C followed by a second staining step with anti-CD127-FITC (clone A7R34, eBioscience), anti-CD103-PE (clone 2E7, eBioscience), anti-CD69-PerCP (clone H1.2F3, BD Biosciences), anti-KLRG1-PE-Cy7 (clone 2F1, eBioscience), anti-CD8a-Pacific-Blue (clone 53-6.7, BD Biosciences) and anti-CD45.2-APC-Cy7 (clone 104, Biolegend). For intravascular staining mice were injected with 3 µg anti-CD45-BV510 (clone 30-F11, Biolegend) intravenously and were killed 3 min later with an overdose of inhaled isoflurane.

Influenza infections

Mice were experimentally infected with 10^4 PFU of H1N1 A/Puerto Rico/8/1934, pH1N1 A/Hamburg/4/2009,[65] H3N2 A/Hong Kong/1/1968 (kindly provided by Prof. Georg Kochs, University Hospital Freiburg, Germany) or H7N7 A/Seal/Massachusetts/1/1980 (SC35M, kindly provided by Prof. Martin Schwemmle, University Hospital Freiburg, Germany). The inoculum was given intranasally under general anesthesia. Mice were killed if they had lost more than 25 % of their initial body weight and did not gain weight again within 48 h. Mice that lost more than 30 % of their initial body weight were also killed with an overdose of inhaled isoflurane. BALF were obtained to analyze tissue damage, viral replication and cellular infiltration. Tissue destruction was determined by detecting total protein in cell-free BALF using bicinchoninic acid assay (Pierce) and the viral RNA was quantified by qRT-PCR as described elsewhere.[64] The detection limit was 3300 copies/ml BALF.

To inhibit circulation of memory T cells, mice were treated with 1 mg/kg FTY720 (Sigma) i.p. daily. The treatment began 3 days before and was maintained throughout the infection.

Flow cytometric analyses of cellular infiltration

BALF from infected mice were centrifuged (5 min, 5000×*g*) and one quarter of the cellular fraction was stained with anti-Gr1-FITC (clone RB6-8C5, eBioscience), anti-CD49b-PE (clone DX5, eBioscience), anti-CD45-PerCP (clone 30-F11, BD Biosciences), anti-CD19-PE-Cy7 (clone 1D3, BD Biosciences), anti-F4/80-APC (clone BM8, eBioscience), anti-CD11b-APC-Cy7 (clone M1/70, BD Biosciences), anti-CD11c-Pacific-Blue (clone HL3, BD Biosciences), and anti-CD3e-BV510 (clone 145-2C11, BD Biosciences). To analyze the cellular infiltration after the immunization, lymphocytes were isolated from lung tissue as described above. FACS Panel I consisted of anti-CD45-PerCP (clone 30-F11, BD Biosciences), anti-CD19-PE-Cy7 (clone 1D3, BD Biosciences), anti-CD11b-APC-Cy7 (clone M1/70, BD Biosciences), anti-CD11c-Pacific-Blue (clone HL3, BD Biosciences), anti-CD3e-BV510 (clone 145-2C11, BD Biosciences), anti-CD4-FITC (clone GK1.5, BD Biosciences), and anti-CD8a-APC (clone 53-6.7, BD Biosciences). Panel II is adapted from Misharin et al.[66] and included anti-I-A/I-E-PerCP (clone M5/114.15.2, Biolegend), anti-Ly6G-PE-Cy7 (clone 1A8, BD Biosciences), anti-CD24-APC (clone M1/69, BD Biosciences), anti-CD11b-APC-Cy7 (clone M1/70, BD Biosciences), anti-Ly6C-Pacific-Blue (clone HK1.4, eBioscience), anti-CD11c-BV510 (HL3, BD Biosciences), anti-CD64-PE (clone X54-5/7.1, Biolegend), and anti-CD45-FITC (30-F11, Biolegend).

Lung-function measurement

Mice were anesthetized and spontaneous breathing was prevented by pancuronium (0.8 mg/kg, i.p.). The trachea was exposed, canulated and connected to a ventilation device (FlexiVent, SCIREQ). The airway resistance (R_N), tissue damping (G), and tissue elastance (H) were investigated at the baseline state and upon vaporization of increasing concentrations of methacholine (0, 6.125, 12.5, 25 mg/ml). Within 2 min after the vaporization of each concentration, five Quick Prime 3 maneuvers were performed.

qRT-PCR analysis of adhesion molecules

Single cell suspensions of lung tissue were obtained as described above and mRNA was isolated using the RNeasy mini kit (Qiagen) and treated with TURBO DNA-free™ kit (Thermo Scientific). Transcriptional levels of reference and adhesion molecule genes were quantified using QuantiTect Probe RT-PCR kit (Qiagen) with SYBR-Green. The following primers were used: *Ubc* for 5′-GCCCAGTGTTACCACCAAGA-3, rev 5′-CCCATCACACCCAAGAACA-3′; *Eef2* for 5′-ATCGCTGAACGCATCAAGC-3′, rev 5′-TGCGCTGGAAGGTCTGGTA-3′; *Vcam1* for 5′-AGTTGGG-GATTCGGTTGTTCT-3′, rev 5′-CCCCTCATTCCTTACCACCC-3′; *Sele* for 5′-AGCCTGCCATGTGGTTGAAT-3′, rev 5′-CTTTGCAT-GATGGCGTCTCG-3′; *Selp* for 5′-AGTGTGACGCTGTGCAATGT-3′, rev 5′-AGGTTGGCAGTGGTTCACTC-3′. Transcriptional levels of target genes were normalized with the geometric mean of *Ubc* and *Eef2*.

Cytokine analyses

Cytokine and chemokine concentrations in cell-free BALF were determined using a Mouse Luminex Screening Assay (R&D Systems) and analyzed on a Luminex 100™ IS system (Luminex Corporation) according to the manufacturer's instructions. A Mouse TGF-beta1 Platinum ELISA kit (eBioscience) was used for measurement of TGFβ in BALF.

Statistical analyses

Results are shown as mean ± SEM or in log-scale figures as median ± interquartile range. Unpaired two-tailed Student's *t*-test and one-way ANOVA with Tukey's post test were performed with Prism 5.0 (GraphPad Software, Inc.). A p value of <0.05 was considered to be statistically significant.

ACKNOWLEDGEMENTS

This work was supported by grants from the German Research Foundation (RTG1949/1) and by intramural research funding from the Ruhr University Bochum (F787R-2013). We thank Klaus Sure, Andrea Wiechers, Bettina Tippler, and Mechthild Hemmler-Roloff for technical assistance. The funders had no role in study design, data collection and analysis, decision to publish, or preparation of the manuscript.

AUTHOR CONTRIBUTIONS

D.L. and M.T. designed and conceived the study. D.L., M.S.B., A.M., V.S., V.H., K.W., and R.H. conducted the experiments. A.M.W., W.B., and C.E contributed reagents and methodical support. D.L. and M.T. analyzed the data and wrote the manuscript. All authors critically revised the manuscript before submission.

ADDITIONAL INFORMATION

The online version of this article (https://doi.org/10.1038/s41385-018-0017-4) contains supplementary material, which is available to authorized users.

Competing interests: The authors declare no competing interests.

REFERENCES

1. World Health Organization Influenza (seasonal). *Fact Sheet No. 211*. http://www.who.int/mediacentre/factsheets/fs211/en/ (2009).
2. Beyer, W. E. P. et al. Cochrane re-arranged: support for policies to vaccinate elderly people against influenza. *Vaccine* **31**, 6030–6033 (2013).
3. Ohmit, S. E. et al. Influenza vaccine effectiveness in the community and the household. *Clin. Infect. Dis.* **56**, 1363–1369 (2013).
4. Skowronski, D. et al. Interim estimates of 2014/15 vaccine effectiveness against influenza A(H3N2) from Canada's sentinel physician surveillance network, January 2015. *Eurosurveillance* **20**, 21022 (2015).
5. Renegar, K. B., Small, P. A., Boykins, L. G. & Wright, P. F. Role of IgA versus IgG in the control of influenza viral infection in the murine respiratory tract. *J. Immunol.* **173**, 1978–1986 (2004).
6. Gianfrani, C., Oseroff, C., Sidney, J., Chesnut, R. W. & Sette, A. Human memory CTL response specific for influenza A virus is broad and multispecific. *Hum. Immunol.* **61**, 438–52 (2000).
7. Bui, H.-H., Peters, B., Assarsson, E., Mbawuike, I. & Sette, A. Ab and T cell epitopes of influenza A virus, knowledge and opportunities. *Proc. Natl Acad. Sci. USA* **104**, 246–251 (2007).
8. Assarsson, E. et al. Immunomic analysis of the repertoire of T-cell specificities for influenza A virus in humans. *J. Virol.* **82**, 12241–12251 (2008).
9. Schulman, J. L. & Kilbourne, E. D. Induction of partial specific heterotypic immunity in mice by a single infection with influenza A virus. *J. Bacteriol.* **89**, 170–4 (1965).
10. Liang, S., Mozdzanowska, K., Palladino, G. & Gerhard, W. Heterosubtypic immunity to influenza type A virus in mice. Effector mechanisms and their longevity. *J. Immunol.* **152**, 1653–61 (1994).
11. Powell, T. J. et al. Priming with cold-adapted influenza a does not prevent infection but elicits long-lived protection against supralethal challenge with heterosubtypic virus. *J. Immunol.* **178**, 1030–1038 (2007).
12. Lanthier, P. A. et al. Live attenuated influenza vaccine (LAIV) impacts innate and adaptive immune responses. *Vaccine* **29**, 7849–7856 (2011).
13. Sridhar, S. et al. Cellular immune correlates of protection against symptomatic pandemic influenza. *Nat. Med.* **19**, 1305–1312 (2013).
14. Hayward, A. C. et al. Natural T cell–mediated protection against seasonal and pandemic influenza. Results of the flu watch cohort study. *Am. J. Respir. Crit. Care Med.* **191**, 1422–1431 (2015).
15. Anderson, K. G. et al. Cutting edge: intravascular staining redefines lung CD8 T cell responses. *J. Immunol.* **189**, 2702–2706 (2012).
16. Wu, T. et al. Lung-resident memory CD8 T cells (TRM) are indispensable for optimal cross-protection against pulmonary virus infection. *J. Leukoc. Biol.* **95**, 215–224 (2014).
17. Zens, K. D., Chen, J. K. & Farber, D. L. Vaccine-generated lung tissue-resident memory T cells provide heterosubtypic protection to influenza infection. *JCI Insight* **1**, e85832 (2016).
18. Iwasaki, A. & Pillai, P. S. Innate immunity to influenza virus infection. *Nat. Rev. Immunol.* **14**, 315–28 (2014).
19. Ichinohe, T., Lee, H. K., Ogura, Y., Flavell, R. & Iwasaki, A. Inflammasome recognition of influenza virus is essential for adaptive immune responses. *J. Exp. Med.* **206**, 79–87 (2009).
20. Pang, I. K., Ichinohe, T. & Iwasaki, A. IL-1R signaling in dendritic cells replaces pattern-recognition receptors in promoting CD8$^+$ T cell responses to influenza A virus. *Nat. Immunol.* **14**, 246–53 (2013).
21. Pober, J. S. & Sessa, W. C. Evolving functions of endothelial cells in inflammation. *Nat. Rev. Immunol.* **7**, 803–815 (2007).
22. Furuichi, K. et al. Interleukin-1-dependent sequential chemokine expression and inflammatory cell infiltration in ischemia-reperfusion injury. *Crit. Care Med.* **34**, 2447–2455 (2006).
23. La Gruta, N. L., Kedzierska, K., Stambas, J. & Doherty, P. C. A question of self-preservation: immunopathology in influenza virus infection. *Immunol. Cell Biol.* **85**, 85–92 (2007).
24. Dinarello, C. A. Immunological and inflammatory functions of the interleukin-1 family. *Annu. Rev. Immunol.* **27**, 519–50 (2009).
25. Ben-Sasson, S. Z. et al. IL-1 acts directly on CD4 T cells to enhance their antigen-driven expansion and differentiation. *Proc. Natl Acad. Sci. USA* **106**, 7119–24 (2009).
26. Ben-Sasson, S. Z. et al. IL-1 enhances expansion, effector function, tissue localization, and memory response of antigen-specific CD8 T cells. *J. Exp. Med.* **210**, 491–502 (2013).
27. Komai-Koma, M. et al. Chemoattraction of human T cells by IL-18. *J. Immunol.* **170**, 1084–90 (2003).
28. Nakanishi, K., Yoshimoto, T., Tsutsui, H. & Okamura, H. Interleukin-18 regulates both Th1 and Th2 responses. *Annu. Rev. Immunol.* **19**, 423–74 (2001).
29. Okamoto, I., Kohno, K., Tanimoto, T., Ikegami, H. & Kurimoto, M. Development of CD8+ effector T cells is differentially regulated by IL-18 and IL-12. *J. Immunol.* **162**, 3202–11 (1999).
30. Hoshino, T. et al. Cutting edge: IL-18-transgenic mice: in vivo evidence of a broad role for IL-18 in modulating immune function. *J. Immunol.* **166**, 7014–8 (2001).
31. Marshall, D. J. et al. Interleukin-18 enhances Th1 immunity and tumor protection of a DNA vaccine. *Vaccine* **24**, 244–253 (2006).
32. Iwai, Y. et al. An IFN-γ-IL-18 signaling loop accelerates memory CD8+ T cell proliferation. *PLoS ONE* **3**, e2404 (2008).
33. Kayamuro, H. et al. Interleukin-1 family cytokines as mucosal vaccine adjuvants for induction of protective immunity against influenza virus. *J. Virol.* **84**, 12703–12 (2010).
34. Lee, Y.-T. et al. Environmental and antigen receptor-derived signals support sustained surveillance of the lungs by pathogen-specific cytotoxic T lymphocytes. *J. Virol.* **85**, 4085–4094 (2011).
35. Mackay, L. K. et al. The developmental pathway for CD103+ CD8+ tissue-resident memory T cells of skin. *Nat. Immunol.* **14**, 1294–1301 (2013).
36. Mandala, S. et al. Alteration of lymphocyte trafficking by sphingosine-1-phosphate receptor agonists. *Science* **296**, 346–9 (2002).
37. Kolb, M., Margetts, P. J., Anthony, D. C., Pitossi, F. & Gauldie, J. Transient expression of IL-1β induces acute lung injury and chronic repair leading to pulmonary fibrosis. *J. Clin. Invest.* **107**, 1529–1536 (2001).
38. Ganter, M. T. et al. Interleukin-1 causes acute lung injury via v 5 and v 6 integrin-dependent mechanisms. *Circ. Res.* **102**, 804–812 (2008).
39. Maaske, A. et al. Mucosal expression of DEC-205 targeted allergen alleviates an asthmatic phenotype in mice. *J. Control. Release* **237**, 14–22 (2016).
40. Mackay, L. K. et al. T-box transcription factors combine with the cytokines TGF-β and IL-15 to control tissue-resident memory T cell fate. *Immunity* **43**, 1101–1111 (2015).
41. Schenkel, J. M. et al. Resident memory CD8 T cells trigger protective innate and adaptive immune responses. *Science* **346**, 98–101 (2014).
42. Krammer, F. & Palese, P. Advances in the development of influenza virus vaccines. *Nat. Rev. Drug Discov.* **14**, 167–182 (2015).
43. Hoft, D. F. et al. Live and inactivated influenza vaccines induce similar humoral responses, but only live vaccines induce diverse T-cell responses in young children. *J. Infect. Dis.* **204**, 845–53 (2011).
44. Shiver, J. W. et al. Replication-incompetent adenoviral vaccine vector elicits effective anti-immunodeficiency-virus immunity. *Nature* **415**, 331–335 (2002).
45. Sullivan, N. J. et al. Accelerated vaccination for Ebola virus haemorrhagic fever in non-human primates. *Nature* **424**, 681–684 (2003).
46. Yang, T. C., Dayball, K., Wan, Y. H. & Bramson, J. Detailed analysis of the CD8+ T-cell response following adenovirus vaccination. *J. Virol.* **77**, 13407–13411 (2003).
47. Barefoot, B. et al. Comparison of multiple vaccine vectors in a single heterologous prime-boost trial. *Vaccine* **26**, 6108–6118 (2008).

48. Garlanda, C., Dinarello, C. A. & Mantovani, A. The interleukin-1 family: back to the future. *Immunity* **39**, 1003–1018 (2013).
49. Lee, J. et al. Differences in signaling pathways by IL-1beta and IL-18. *Proc. Natl Acad. Sci. USA* **101**, 8815–20 (2004).
50. Dinarello, C. A. Biologic basis for interleukin-1 in disease. *Blood* **87**, 2095–147 (1996).
51. Knudson, C. J., Weiss, K. A., Hartwig, S. M. & Varga, S. M. The pulmonary localization of virus-specific T lymphocytes is governed by the tissue tropism of infection. *J. Virol.* **88**, 9010–9016 (2014).
52. Teijaro, J. R. et al. Cutting edge: tissue-retentive lung memory CD4 T cells mediate optimal protection to respiratory virus infection. *J. Immunol.* **187**, 5510–5514 (2011).
53. Eliasson, D. G. et al. M2e-tetramer-specific memory CD4 T cells are broadly protective against influenza infection. *Mucosal Immunol.* https://doi.org/10.1038/mi.2017.14 (2017).
54. Jones, M. R., Simms, B. T., Lupa, M. M., Kogan, M. S. & Mizgerd, J. P. Lung NF- B activation and neutrophil recruitment require IL-1 and TNF receptor signaling during *Pneumococcal pneumonia*. *J. Immunol.* **175**, 7530–7535 (2005).
55. Miller, L. S. et al. Inflammasome-mediated production of IL-1 is required for neutrophil recruitment against *Staphylococcus aureus* in vivo. *J. Immunol.* **179**, 6933–6942 (2007).
56. Wakim, L. M., Smith, J., Caminschi, I., Lahoud, M. H. & Villadangos, J. A. Antibody-targeted vaccination to lung dendritic cells generates tissue-resident memory CD8 T cells that are highly protective against influenza virus infection. *Mucosal Immunol.* **8**, 1060–1071 (2015).
57. Casey, K. A. et al. Antigen-independent differentiation and maintenance of effector-like resident memory T cells in tissues. *J. Immunol.* **188**, 4866–75 (2012).
58. Shin, H. & Iwasaki, A. A vaccine strategy that protects against genital herpes by establishing local memory T cells. *Nature* **491**, 463–7 (2012).
59. Takamura, S. et al. Specific niches for lung-resident memory CD8+ T cells at the site of tissue regeneration enable CD69-independent maintenance. *J. Exp. Med.* **213**, 3057–3073 (2016).
60. He, T. C. et al. A simplified system for generating recombinant adenoviruses. *Proc. Natl Acad. Sci. USA* **95**, 2509–14 (1998).
61. Park, S. H. et al. Generation and application of new rat monoclonal antibodies against synthetic FLAG and OLLAS tags for improved immunodetection. *J. Immunol. Methods* **331**, 27–38 (2008).
62. Reed, L. J. & Muench, H. A simple method of estimating fifty per cent endpoints. *Am. J. Hyg.* **27**, 493–497 (1938).
63. Tenbusch, M. et al. Codon-optimization of the hemagglutinin gene from the novel swine origin H1N1 influenza virus has differential effects on CD4(+) T-cell responses and immune effector mechanisms following DNA electroporation in mice. *Vaccine* **28**, 3273–7 (2010).
64. Stab, V. et al. Protective efficacy and immunogenicity of a combinatory DNA vaccine against influenza A virus and the respiratory syncytial virus. *PLoS ONE* **8**, e72217 (2013).
65. Seyer, R. et al. Synergistic adaptive mutations in the hemagglutinin and polymerase acidic protein lead to increased virulence of pandemic 2009 H1N1 influenza A virus in mice. *J. Infect. Dis.* **205**, 262–271 (2012).
66. Misharin, A. V., Morales-Nebreda, L., Mutlu, G. M., Budinger, G. R. S. & Perlman, H. Flow cytometric analysis of macrophages and dendritic cell subsets in the mouse lung. *Am. J. Respir. Cell Mol. Biol.* **49**, 503–510 (2013).